Materials & Design 205 (2021) 109771

Contents lists available at ScienceDirect

Materials & Design

journal homepage: www.elsevier.com/locate/matdes

Ultrasonic injection molding of glass fiber reinforced polypropylene parts using tungsten carbide-cobalt mold core

Xiong Liang, Yongjing Liu, Zehang Liu, Jiang Ma, Zhenxuan Zhang, Wenqing Ruan, Shuai Ren, Taijiang Peng, Xiaoyu Wu, Hongyan Shi *

Shenzhen Key Laboratory of High Performance Nontraditional Manufacturing, College of Mechatronics and Control Engineering, Shenzhen University, Shenzhen 518060, China

ARTICLE INFO

Article history:
Received 27 January 2021
Revised 18 April 2021
Accepted 23 April 2021
Available online 27 April 2021

Keywords:
Ultrasonic injection molding
Tungsten carbide-cobalt
Replication rate
Wettability
Mechanical properties

ABSTRACT

A hybrid process combining ultrasonic injection molding and electrical discharge machining was proposed to realize the economic, high-precision, and environmental-friendliness production of glass fiber reinforced polypropylene microstructured parts. First, the prism array microstructures were processed on tungsten carbide-cobalt (WC-8 wt% Co) substrate by low-speed wire electrical discharge machining and used as the mold core. Then, the glass fiber reinforced polypropylene composite (GF/PP) was melted under ultrasonic vibration, and the surface microstructure of the mold core was replicated. The experimental results show that this method can efficiently and accurately manufacture microstructured parts, and the microstructure has a high replication rate up to 95.5%. By replicating the microstructure, the surface contact angle of GF/PP parts increased from 57.1° to 134.9°, and the wettability changed from hydrophilicity to hydrophobicity. The mechanical properties test results show that the GF/PP parts fabricated by ultrasonic injection molding had excellent mechanical properties, and the 30% GF/PP parts show the highest tensile strength of 56.9 MPa. This work provides a new option for fabricating fiber reinforced composite parts.

1. Introduction

In the trend of product miniaturization, micromachining technology has been further developed. Typical micromachining techniques include precision turning, micro-milling, precision grinding, and micro-electrical discharge machining [1]. These micromachining techniques have been widely applied in micro-electromechanical systems, aviation, automotive, and biomedical engineering due to their low energy consumption, high material utilization, high production efficiency and near-net-shape characteristic [2–4]. Processing ordered array microstructures on the surface of material can make the material obtain many valuable properties, such as wettability [5], antibacterial [6], optical properties [7], and these ordered microstructures with special functions have attracted great interest in research. Micromachining technology is particularly suitable for the fabrication of array microstructures due to its high dimensional accuracy and the ability to process complex shapes.

Polymers are widely selected as raw materials for micro parts because of their low cost, light weight, and excellent machinability. Conventional polymer parts molding process mainly includes hot embossing [8], injection molding [9], and extrusion [10]. When fabricating large size parts, these processes have highly molding efficient and can achieve mass production. However, when the size of parts is small, such as micron level, these methods appear to be somewhat unsatisfactory, prone to defects such as difficult filling, low dosage accuracy, high material waste, and low dimensional accuracy. Therefore, it is necessary to develop processing methods suitable for polymer micro molding.

Power ultrasonics uses the energy of ultrasonic vibrations to change some properties of an object [11]. Ultrasonic energy is widely used in welding processes because it can instantly soften the polymer surface for fast bonding [12]. By taking advantage of this characteristic of ultrasound, the ultrasonic injection molding process has been developed. Compared with conventional hot embossing, ultrasonic injection molding does not require repeated heating and cooling of the mold, which significantly improves productivity; compared with injection molding, it does not have a complex flow channel design and does not require external heating devices, reducing material and energy consumption [13]. Masato et al. [14] compared the ultrasonic injection molding process with the conventional injection molding process. The overall mechanical properties of the samples obtained by the ultrasonic injection

* Corresponding author.
E-mail address: shihongyan@szu.edu.cn (H. Shi).

https://doi.org/10.1016/j.matdes.2021.109771
0264-1275/

molding process were not only comparable to those of the samples obtained by the injection molding process, but even exhibited significant improvement. Masato et al. concluded that the ultrasonic injection molding process is an effective alternative to the conventional method. Liang et al. [15,16] analyzed the surface morphologies of samples fabricated at different process parameters, and obtained the influence of process parameters on the quality of plastic parts. Sanchez-Sanchez et al. [17] fabricated UHMWPE tensile specimens by ultrasonic injection molding process and investigated the effects of process parameters on the structure, degradation, and mechanical properties of UHMWPE. Jiang et al. [18] investigated the flow characteristics of polymer melts and their filling capacity under the parameters of ultrasonic amplitude, ultrasonic action time, plasticizing pressure, and mold temperature. They concluded that ultrasonic injection molding was useful in filling high-aspect ratio microcavities.

The successful application of ultrasonic injection molding has provided more options for processing polymer materials. Glass fibers reinforced polypropylene composite (GF/PP) is a material with excellent properties and generally used to replace wood and steel [19]. Compared with pure polypropylene, its mechanical strength, rigidity, impact strength, creep resistance and fatigue resistance show better mechanical properties; Compared with metal materials, it has the characteristics of low density, light weight, high specific strength, corrosion resistance and easy molding [20]. These excellent properties indicate its broad application prospects. However, there are few reports on methods for processing GF/PP composite microparts.

In this work, an ultrasonic injection molding process using low-speed wire electrical discharge machining (WEDM-LS) machined mold cores was presented to obtain GF/PP parts. Optimal process parameters for ultrasonic injection molding were used to replicate the microstructure of the mold core surface to the polymer composite surface. The static contact angle (CA) was evaluated the wettability of the replicated polymer composite surface. The mechanical properties and replication capability of GF/PP parts fabricated by ultrasonic injection molding process was investigated. As well be revealed, the fabrication of composite microstructured parts by ultrasonic injection molding is a high-precision, economic and environmentally friendly method with potential applications prospects.

2. Experimental details

2.1. Materials

The raw material was glass fiber reinforced polypropylene (GF/PP) produced by Hanwha Total Petrochemical Co., Ltd., and the glass fiber content was 10%, 20% and 30%, respectively.

The raw material of the mold core is WC-8 wt% Co composite produced by Zhuzhou Cemented Carbide Group Co., Ltd., China. This material is an ideal die material because of its excellent mechanical properties such as high hardness, good thermal stability and high precision.

2.2. Design and processing of mold core

WEDM-LS is widely used in the field of difficult-to-machine materials because there is no mechanical force between workpiece and electrode in the machining process [21]. Therefore, WEDM-LS is one of the effective methods for processing WC-8 wt% Co mold core.

Fig. 1 shows the process of mold core by WEDM-LS (AP250LS, Sodick, Japan). During the machining process, a brass wire with a diameter of 100 μm was discharged to the WC-8 wt% Co substrate according to a predetermined path. Oil-based dielectric fluid provides a machining environment free of outside air, preventing external oxygen from affecting the machined surface and taking away the machining debris. To improve the surface quality of the die core, a multi-cutting method must be used to process the workpiece, with rough cutting first, followed by trim cutting at low energy.

2.3. Ultrasonic injection molding process

Fig. 2 shows a schematic of the ultrasonic injection molding process. Ultrasonic injection molding of GF/PP was performed on an ultrasonic welding machine (2000XCT, Branson, USA). The machine delivers ultrasonic waves at a frequency of 20 kHz with a maximum output of 2500 W. The ultrasonic injection molding process consists of preparation work, ultrasonic plasticizing, packing stage, and demolding. First, the mold is assembled and fixed onto the machine platform, and the charging barrel hole in the upper plate is filled with a certain mass of GF/PP pellets. Second, set parameters on the control panel, then start the ultrasonic welding machine. GF/PP pellets melted under the action of ultrasonic vibration, and the melt filled into the mold cavity with the downward movement of the ultrasonic sonotrode. Finally, the melt is cooled under a certain pressure, and the GF/PP part is removed from the mold. The process parameters are listed in Table 1.

2.4. Characterization

The surface topography of the mold core and microstructured parts was obtained by scanning electron microscopy (SEM, Quanta FEG450, FEI, USA). The instrument was also used to observe the fracture topography of the tensile specimens. Because the specimens are non-conductive materials, they were gold-sprayed before observation. The three-dimensional morphology and dimensional data of the mold core and microstructured parts were obtained by a laser scanning confocal microscope (VK-X250K, Keyence, Japan).

The tensile specimens were tested at room temperature using a universal material testing machine (Z050, ZwickRoell, Germany). The specimens were non-standard tensile specimens, fixed using custom-made fixtures, and tensile speeds is 2 mm/min. To ensure the reliability of the data, the samples with different glass fiber contents were tested five times and the final data were composed of the average and deviation of the measured data.

The CA of the microstructure surface was measured using a droplet shape analyzer (DSA100S, Krüss, Germany). The measurement liquid was deionized water with a volume of 2 μL, and the measurement method was the sessile drop method [22]. The surface of each microstructured part was measured at three different positions, and the averages of the measured data were taken as the final data.

3. Results and discussion

3.1. Surface morphology of mold core

As shown in Fig. 3, the WC-8 wt% Co mold core with prism array microstructures on the surface were processed by controlling the motion trajectory of the wire electrode. The width and height of the single prism are 123.15 ± 0.59 μm and 193.17 ± 0.31 μm respectively, and the spacing between the prisms is 156.18 ± 0.57 μm. It can be observed in the partial amplification diagram that sub-micron discharge pits generated by spark discharge corrosion are distributed on the surface of the mold core. After measurement, the upper and lower surface roughness Ra of the microstructure

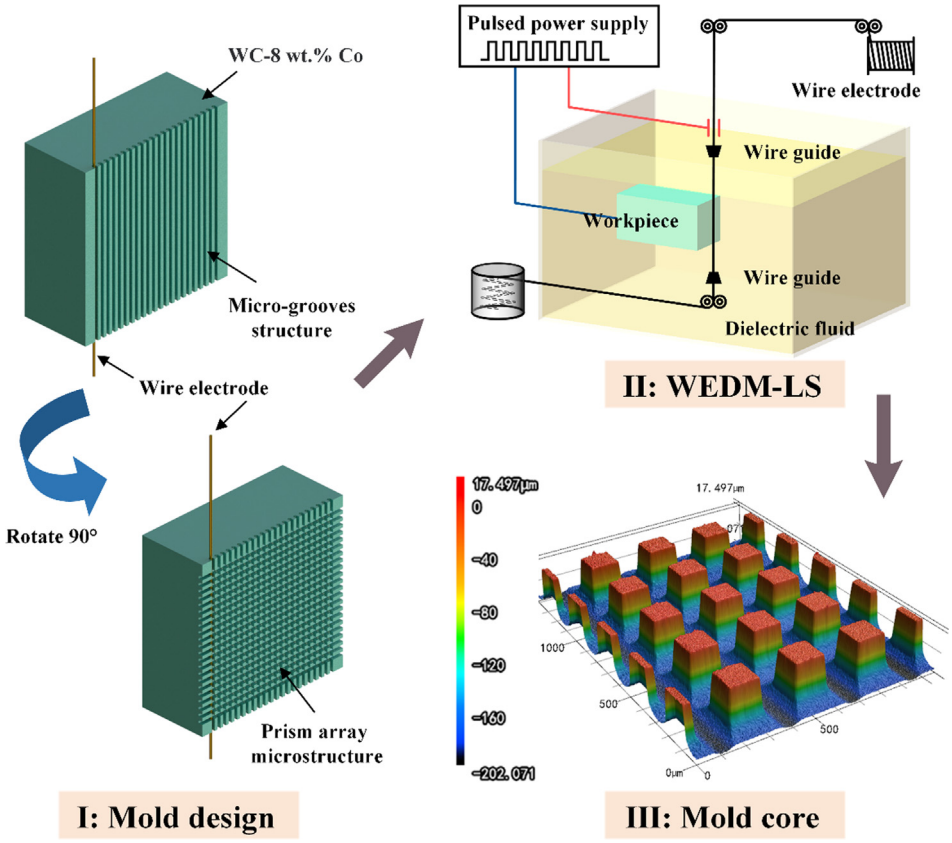

Fig. 1. Design and processing of mold core.

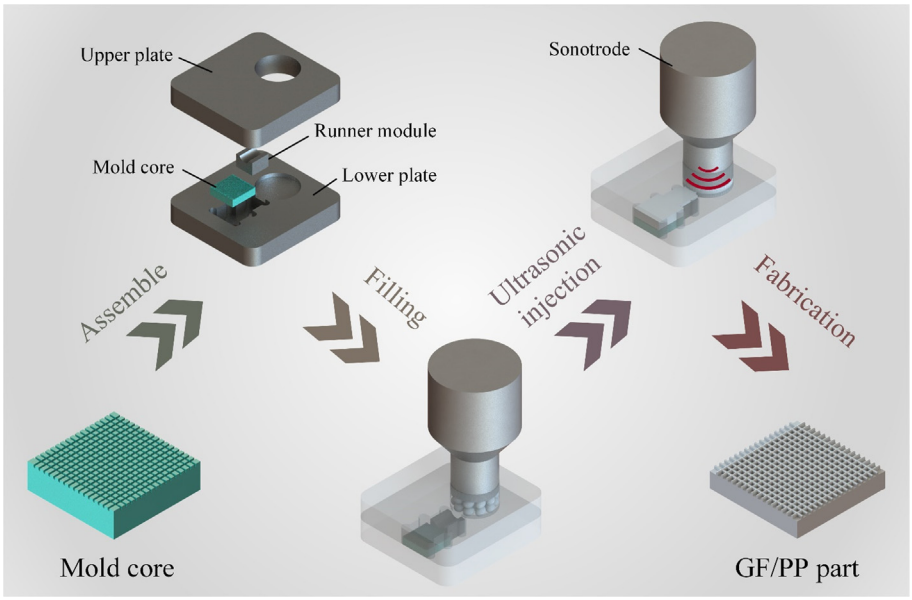

Fig. 2. Schematic diagram of ultrasonic injection molding process.

Table 1
Process parameters for ultrasonic injection molding.

Process parameter	Ultrasonic energy (J)	Weld pressure (kPa)	Hold time (s)	Amplitude (μm)
Values	600/900/1200	110	8	37.5

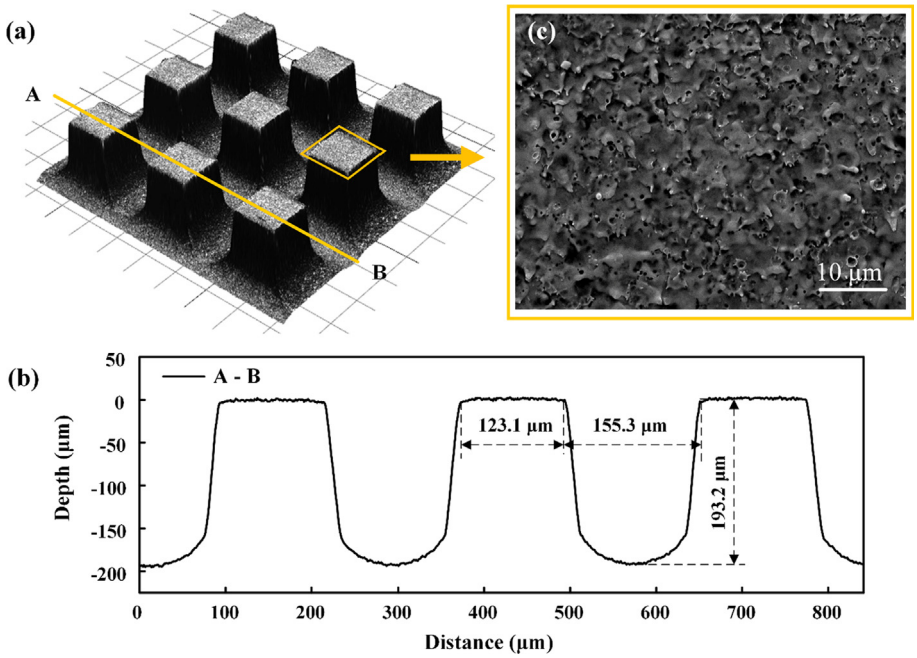

Fig. 3. The WC-8 wt% mold core: (a) prism array microstructure; (b) the cross-sections profile of mold; (c) the surface morphology of mold after WEDM-LS.

are 0.43 μm and 1.24 μm, respectively. The surface quality of the lower surface is lower than that of the upper surface due to the structural limitation of the cylindrical wire electrode and the influence of concentrated discharge [23], so the roughness of the upper and lower surfaces is inconsistent.

3.2. Microstructure replication by GF/PP ultrasonic injection molding.

The WC-8 wt% Co with prism array microstructure described in the above section is used as the mold core, and the 30% GF/PP pellets were used to replicate the microstructure from mold core by ultrasonic injection molding. Fig. 4a shows the GF/PP microstructured part fabricated under different ultrasonic energy. When the ultrasonic energy was 600 J, only a small amount of melt filled into the gap between the prisms, and the height of the rectangular grid microstructure on the surface of the GF/PP part was low. When the ultrasonic energy increases to 800 J, more melt filled into the gap between the prisms, the surface microstructure of the GF/PP part was visible, and the height of the microstructure increased. When the ultrasonic energy was 1200 J, the gap between the prisms was filled, and the surface rectangular grid array microstructure of the GF/PP part was clear and complete.

Insufficient ultrasonic energy can only melt a small part of GF/PP pellets, and most GF/PP pellets are only bonded together in the mold cavity. At this time, there are clear pellet boundaries and large voids on the surface. Therefore, the microstructure of the mold core surface is not replicated completely. Sufficient ultrasonic energy makes the GF/PP pellets melt in a short time, and the macromolecules have enough freedom of movement in the molten state, which is beneficial to the melt flowing into the mold cavity. At the same time, the 20 kHz high-frequency ultrasonic vibration excited the diffusion and interpenetration of the chain at the interface [24], which makes the fabricated GF/PP parts with a stable welding effect (Fig. 4b).

In order to evaluate the forming quality of the GF/PP parts, the surface roughness and microstructure depth of GF/PP parts are the main criterion. The upper surface roughness Ra of GF/PP parts was 0.94 μm, and the lower surface roughness Ra was 0.62 μm, which are lower than the mold core machined by WEDM-LS. An α parameter, which describes the replication rate of GF/PP part surface microstructure under the ultrasonic injection molding process, is proposed as:

$$\alpha = \frac{H_1}{H_2} \times 100\% \quad (1)$$

where H_1 is the height of the GF/PP microstructure and H_2 is the height of the prism of the mold core (Fig. 4d). Fig. 4c shows the height measurement results of the surface microstructure of 10 GF/PP parts, and the mean value of heights is 184.47 ± 1.49 μm. According to formula (1), the calculated α value is 95.5%. The large value of the parameter indicates excellent filling ability during ultrasonic injection.

3.3. Wettability on microstructure surfaces of GF/PP parts

It is well known that the surface wettability of a material is related to its surface structure and activation energy. There, by constructing a microstructure on the material surface, the surface can be made to have a certain wettability [25].

Fig. 5 shows the optical images of the CA on the structure-free surface and rectangular grid microstructure surface. The CA on the structure-free surface was 57.1°, and the CA on the rectangular grid microstructure surface was 134.9°. The measurement results show that the structure-free surface exhibits hydrophilicity, but after constructing the microstructure on the surface, it exhibits good hydrophobic properties. This result indicates that the construction of microstructures on the surface can change the hydrophobicity of the specimen surface. The diffusion and spreading of droplets on a solid surface are related to the surface topography of the solid [26]. As described by Cassie-Baxter model, some air is trapped in the rectangular grid microstructure, and the bottom of the droplet forms a solid–liquid-gas interface, which may give rise to the hydrophobicity of the surface (Fig. 5c). In addition, the movement of the droplets is blocked by the rectangular grid microstructure, and the resistance or energy barrier for the droplets to cross the adjacent grid microstructure is large; therefore, the CA is large than that of the structure-free surface.

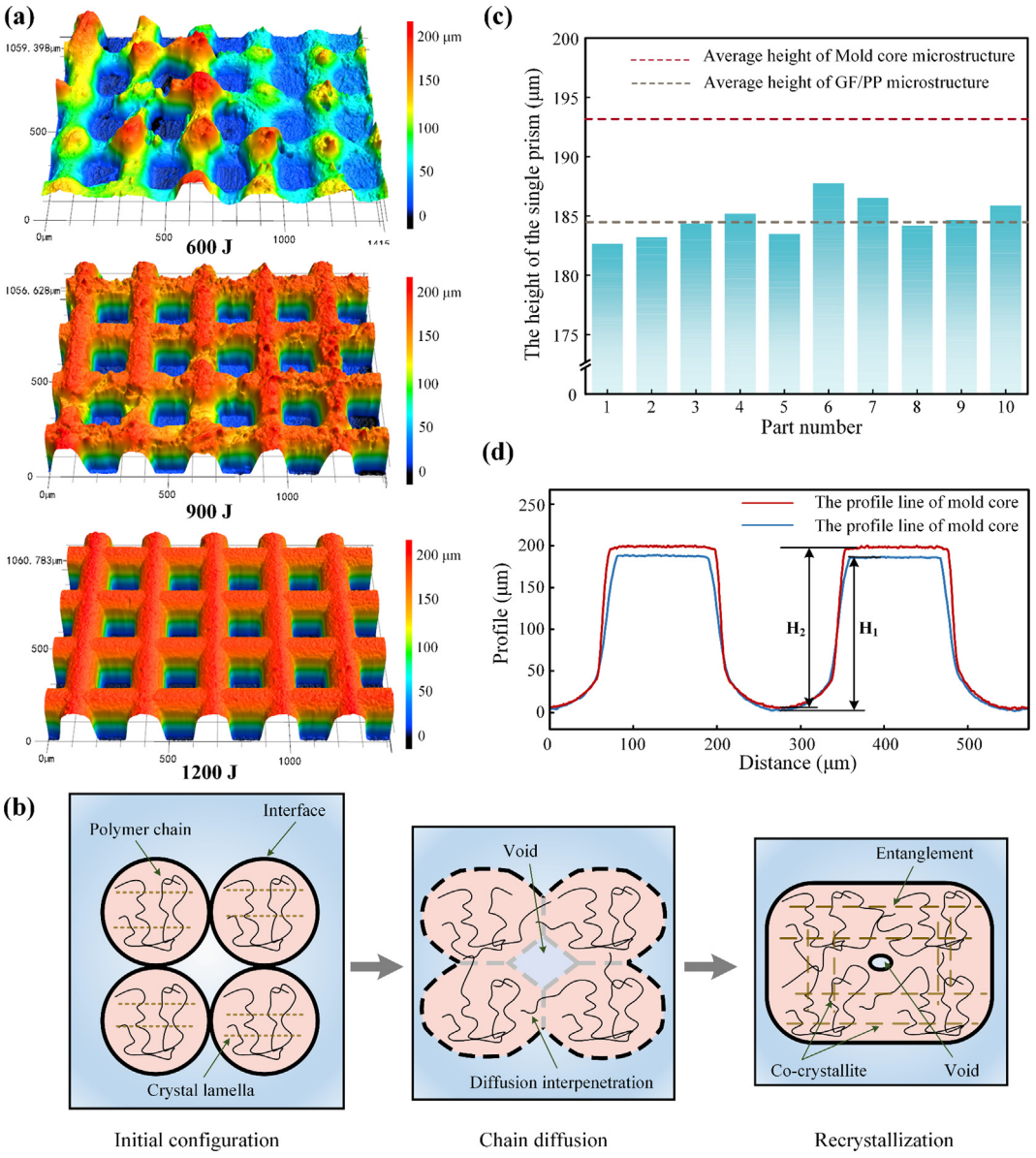

Fig. 4. GF/PP part: (a) surface morphology evolution of GF/PP parts under different ultrasonic energy; (b) process of pellets melting; (c) comparison of microstructure height of GF/PP Parts; (d) cross-sectional profile of mold core microstructure and GF/PP part microstructure.

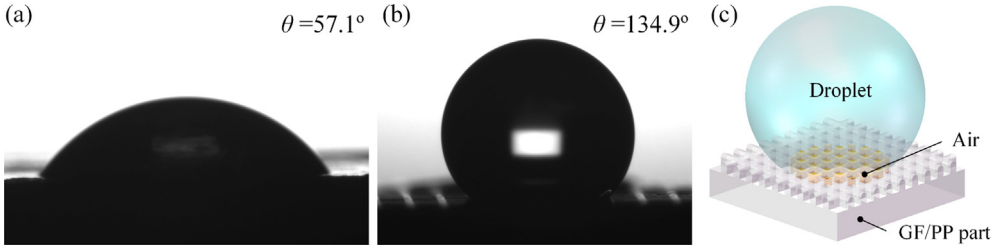

Fig. 5. The optical photos of WCA on GF/PP parts surfaces and model schematic: (a) structure-free surface; (b) rectangular grid microstructure surface; (c) the state of droplets on the surface of the microstructure.

3.4. Mechanical properties

In general, the properties of GF/PP parts are closely related to fiber orientation and content. To investigate the mechanical properties of GF/PP parts fabricated by ultrasonic injection molding process, GF/PP tensile specimens with glass fiber content of 10%, 20%, and 30% were fabricated by using the parameters in the previous section that can completely fabricated GF/PP microstructure parts.

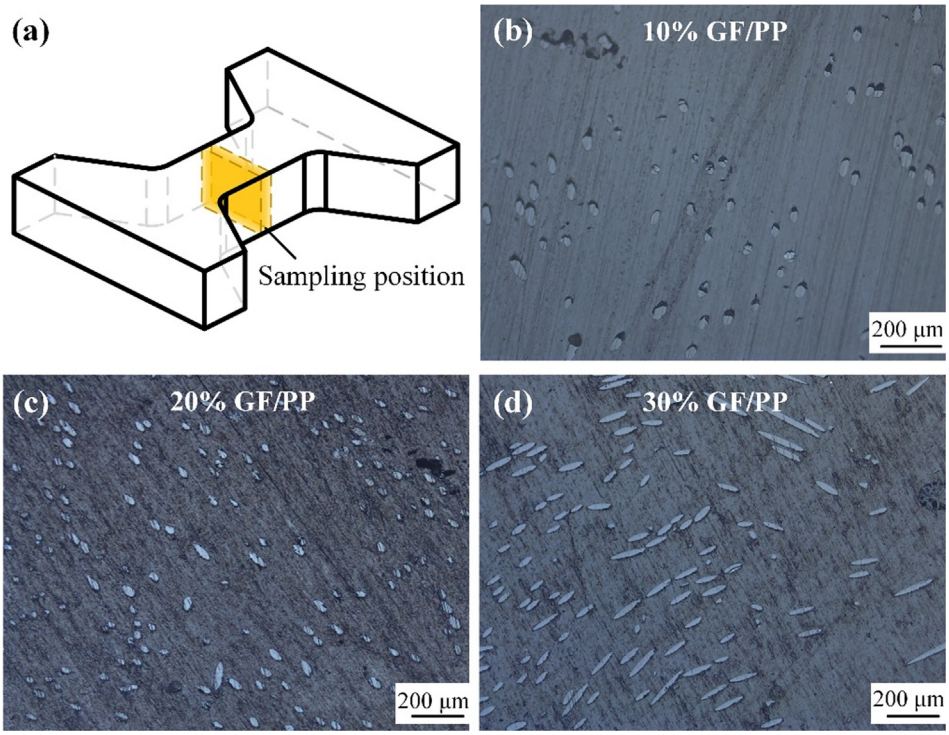

Fig. 6. (a) Sampling position of GF/PP tensile sample, (b)-(d) fiber orientation state of samples with different glass fiber contents.

3.4.1. Orientation of glass fiber

Fig. 6a shows the sampling position of the GF/PP tensile sample. The obtained sample was packaged with resin and then polished. Fig. 6b-d are the cross-sectional microscopic photograph of samples. To facilitate observation, the contrast and grayscale parameters of the photograph were adjusted. When the glass fiber content is 10%, the orientation state of glass fiber is mainly circular cross-section. With the increase of glass fiber content, the circular cross-section in the glass fiber orientation state decreases, the elliptical cross-section increases and the sizes varied. For the above experimental phenomena, the analysis shows that when the glass fiber content is low, the ultrasonic energy mainly acts on the polymer matrix. The ultrasonic vibration enhances the creep of molecular chains and improves the fluidity of the melt, which makes the glass fibers easily oriented along the direction of solution flow. When the glass fiber content is high, the ultrasonic energy directly acts on the glass fiber. The increased kinetic energy causes the change of glass fiber movement. The fiber has a certain tilt rotation in the flow direction of the solution, and the orientation of the glass fiber is weakened, showing an irregular distribution.

3.4.2. Tensile test

Fig. 7a shows the pictures of pure PP and 10%, 20%, and 30% GF/PP tensile samples before and after testing. The tensile strength and elongation at break are recorded in Fig. 7b and Table 2. The fracture process of tensile samples can be divided into three stages. Starting from elastic deformation, it occurs at low load on PP matrix and glass fiber. Then, with the increase of load, cracks first appear on the PP matrix in the middle of the sample, in which glass fiber bears most of the load. Finally, the fiber breaks or pulls out. According to the experimental data, the tensile strength of pure PP is 31.1 MPa. When the glass fiber content is 10%, the tensile strength of the tensile sample is 40.3Mpa, which is about 29.6% higher than that of pure PP. When the glass fiber content is 20%, the tensile strength of the tensile sample is 44.6 MPa. When the glass fiber content is 30%, the tensile strength of the tensile sample reached 56.9 MPa, and the tensile strength is increased by 43.4%. While the elongation at break of tensile samples decreased from 256.7% (pure PP) to 45.5% MPa (30% GF/PP sample). The experimental results show that the glass fibers with high strength properties play a role in skeleton reinforcement, and the tensile strength almost shows a linear growth with the increase of glass fiber content. Since glass fiber is a rigid material with high tensile strength, its limited deformation leads to low elongation at break of GF/PP composites [27]. Therefore, plastic deformation occurred in pure PP tensile specimen during tensile loading, and GF/PP tensile specimen showed brittle fracture.

Fig. 8 shows the SEM image of the tensile fracture surface. It can be seen from the figure that when the glass fiber content is low, glass fiber aggregation occurs and its distribution in the matrix is poor. In addition, the fracture surface is flat and there are more voids, indicating that most glass fibers are pulled out of the matrix during tensile testing. In this case, the glass fiber bears less force. When the glass fiber content is high, the fracture surface is not flat and distributed with the mesh structure formed by the interlacing of glass fibers. During the tensile test, the stress on the sample was transferred from the PP matrix to the glass fiber until the glass fiber broke. Therefore, the tensile strength of the sample is also improved with the increase of glass fiber content.

4. Conclusions

In this study, a method for fabricating GF/PP microstructured parts by ultrasonic injection molding was investigated. The following conclusions are drawn from the experimental results and analysis:

(1) The WC-8 wt% Co with prism array microstructures were processed through WEDM-LS. GF/PP pellets melt under ultrasonic energy and directly replicate the surface microstructure of the mold core. The experimental results show that the smaller ultrasonic energy does not fully melt

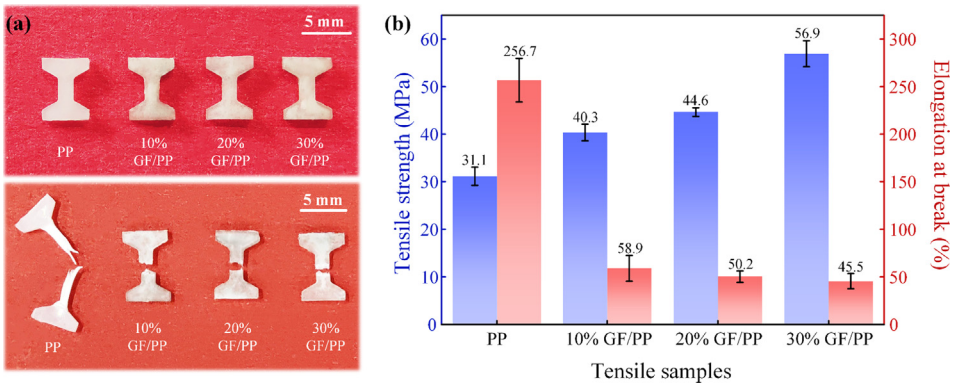

Fig. 7. (a) Tensile samples; (b) tensile strength and elongation at break of tensile samples.

Table 2
Tensile properties.

Glass fiber content (%)	Tensile strength (MPa)	Elongation at break (%)
0	31.14 ± 1.92	256.73 ± 22.85
10	40.34 ± 1.74	58.95 ± 3.21
20	44.64 ± 0.93	50.24 ± 3.15
30	56.92 ± 2.74	45.49 ± 1.93

the material, and the fabricated GF/PP parts are incomplete. The larger ultrasonic energy melts the material sufficiently, and the melt replicate the surface microstructure of the mold core. The replication rate of the microstructured parts is nearly 95.5%, showing excellent replication ability of GF/PP under ultrasonic injection molding.

(2) Using ultrasonic injection molding to fabricate microstructures on the surface, the CA was increased from 57.1° to 134.9° to achieve a transformation from hydrophilic to

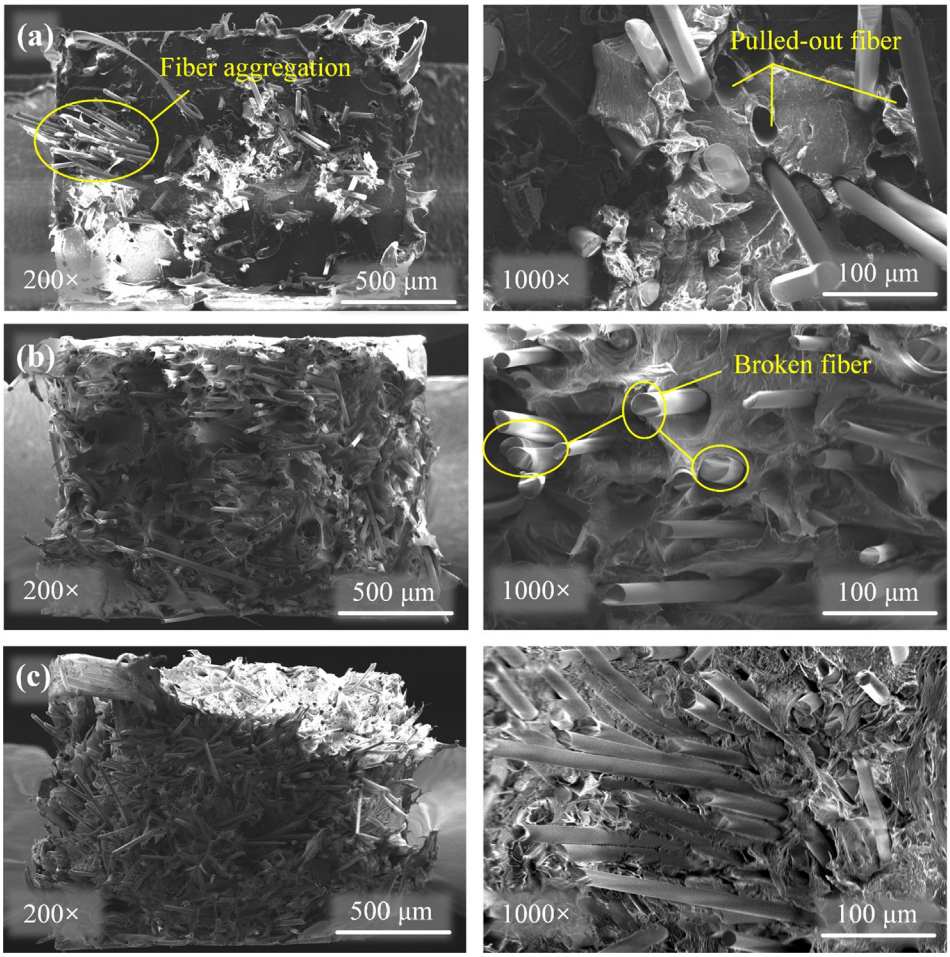

Fig. 8. The SEM images of tensile fracture surface: (a) 10% GF/PP; (b) 20% GF/PP; (c) 30% GF/PP.

hydrophobic surfaces, and this result made it possible for ultrasonic injection molding to fabricate hydrophobic surfaces rapidly.

(3) The mechanical properties of GF/PP parts fabricated by ultrasonic injection molding are closely related to the orientation and content of glass fiber. For the 10% GF/PP sample, the glass fiber was oriented along the direction of the solute flow. With the increase of glass fiber content, the ultrasonic energy directly acts on the glass fiber, resulting in fiber tilt rotation and irregular distribution. The tensile experimental results showed that the tensile strength of 10%, 20% and 30% GF/PP were 40.3 MPa, 44.6 MPa, and 56.9 MPa, and the elongation at break was 58.9%, 50.2%, and 45.5%, respectively. With the increase of glass fiber content, the high strength glass fiber plays a role in skeleton reinforcement, and the tensile strength of the sample almost increases linearly. While glass fiber is a rigid material, its limited deformation variation leads to a relatively low elongation at break.

(4) To optimize the quality and stability of GF/PP ultrasonic injection molding parts, more cycles and thermal properties of GF/PP parts are good indicators. Further research on ultrasonic injection molding of fiber reinforced composites is underway.

Declaration of Competing Interest

The authors declare that they have no known competing financial interests or personal relationships that could have appeared to influence the work reported in this paper.

Acknowledgements

This work was supported in part by the National Natural Science Foundation of China (Nos. 51971150, 51871157 and 52075344), the Natural Science Foundation of Guangdong Province (No. 2016A030310036), the Science, Technology and Innovation Commission of Shenzhen Municipality (Nos. JCYJ20170412111216258 and JSGG20190219152602381).

Data availability

The raw/processed data required to reproduce these findings cannot be shared at this time due to technical or time limitations.

References

[1] N. Chen, H.N. Li, J. Wu, Z. Li, L. Li, G. Liu, N. He, Advances in micro milling: From tool fabrication to process outcomes, Int. J. Mach. Tools Manuf 103670 (2020).
[2] S.K. Chaubey, N.K. Jain, State-of-art review of past research on manufacturing of meso and micro cylindrical gears, Precis. Eng.-J. Int. Soc. Precis. Eng. Nanotechnol. 51 (2018) 702–728.
[3] M.W. Fu, W.L. Chan, A review on the state-of-the-art microforming technologies, Int. J. Adv. Manuf. Technol. 67 (2013) 2411–2437.
[4] J. Lei, X. Wu, Z. Zhou, B. Xu, L. Zhu, Y. Tang, Sustainable mass production of blind multi-microgrooves by EDM with a long-laminated electrode, J. Cleaner Prod. 279 (2021) 123492.
[5] A. Davoudinejad, Y.K. Cai, D.B. Pedersen, X.C. Luo, G. Tosello, Fabrication of micro-structured surfaces by additive manufacturing, with simulation of dynamic contact angle, Mater. Des. 176 (2019) 11.
[6] M.M. Alves, D.V. Cunha, C.F. Santos, N.P. Mira, M.F. Montemor, Microstructured ZnO-rod like coating prevents biofilm formation prompted by pathogenic Candida spp, Ceram. Int. 44 (2018) 4467–4472.
[7] M.T. Wu, B. Guo, Q.L. Zhao, P. He, Precision grinding of a microstructured surface on hard and brittle materials by a microstructured coarse-grained diamond grinding wheel, Ceram. Int. 44 (2018) 8026–8034.
[8] J. Gao, L.F. Peng, Y.J. Deng, P.Y. Yi, Z.Q. Lin, Experimental studies on micro powder hot embossing for high-aspect-ratio microstructures with ultra-high molecular weight polyethylene powders, J. Micromech. Microeng. 30 (2020) 10.
[9] H.Y. Zhang, F.Z. Fang, M.D. Gilchrist, N. Zhang, Precision replication of micro features using micro injection moulding: Process simulation and validation, Mater. Des. 177 (2019) 13.
[10] T. Kunishima, T. Kurokawa, H. Arai, V. Fridrici, P. Kapsa, Reactive extrusion mechanism, mechanical and tribological behavior of fiber reinforced polyamide 66 with added carbodiimide, Mater. Des. 188 (2020) 12.
[11] T. Dorf, K. Perkowska, M. Janiszewska, I. Ferrer, J. Ciurana, Effect of the main process parameters on the mechanical strength of polyphenylsulfone (PPSU) in ultrasonic micro-moulding process, Ultrason. Sonochem. 46 (2018) 46–58.
[12] K.F. Wang, D. Shriver, Y. Li, M. Banu, S.J. Hu, G.X. Xiao, J. Arinez, H.T. Fan, Characterization of weld attributes in ultrasonic welding of short carbon fiber reinforced thermoplastic composites, J. Manuf. Processes 29 (2017) 124–132.
[13] U. Heredia-Rivera, I. Ferrer, E. Vazquez, Ultrasonic Molding Technology: Recent Advances and Potential Applications in the Medical Industry, Polymers 11 (2019) 4.
[14] D. Masato, M. Babenko, B. Shriky, T. Gough, G. Lucchetta, B. Whiteside, Comparison of crystallization characteristics and mechanical properties of polypropylene processed by ultrasound and conventional micro-injection molding, Int. J. Adv. Manuf. Technol. 99 (2018) 113–125.
[15] X. Liang, Y.J. Liu, J. Ma, F. Gong, Y. Lou, L.Y. Fu, B. Xu, Fabrication of Micro Ultrasonic Powder Molding Polypropylene Part with Hydrophobic Patterned Surface, Materials 13 (2020) 13.
[16] X. Liang, Y.J. Liu, S.G. Chen, J. Ma, X.Y. Wu, H.Y. Shi, L.Y. Fu, B. Xu, Fabrication of microplastic parts with a hydrophobic surface by micro ultrasonic powder moulding, J. Manuf. Processes 56 (2020) 180–188.
[17] X. Sanchez-Sanchez, M. Hernandez-Avila, L.E. Elizalde, O. Martinez, I. Ferrer, A. Eliss-Zuniga, Micro injection molding processing of UHMWPE using ultrasonic vibration energy, Mater. Des. 132 (2017) 1–12.
[18] B.Y. Jiang, Y. Zou, T. Liu, W.Q. Wu, Characterization of the Fluidity of the Ultrasonic Plasticized Polymer Melt by Spiral Flow Testing under Micro-Scale, Polymers 11 (2019) 10.
[19] M. Etcheverry, S.E. Barbosa, Glass Fiber Reinforced Polypropylene Mechanical Properties Enhancement by Adhesion Improvement, Materials 5 (2012) 1084–1113.
[20] P. Parandoush, L. Tucker, C. Zhou, D. Lin, Laser assisted additive manufacturing of continuous fiber reinforced thermoplastic composites, Mater. Des. 131 (2017) 186–195.
[21] M.P. Jahan, M. Rahman, Y.S. Wong, A review on the conventional and micro-electrodischarge machining of tungsten carbide, Int. J. Mach. Tools Manuf. 51 (2011) 837–858.
[22] M. Ijavi, R.W. Style, L. Emmanouilidis, A. Kumar, S.M. Meier, A.L. Torzynski, F.H. T. Allain, Y. Barral, M.O. Steinmetz, E.R. Dufresne, Surface tensiometry of phase separated protein and polymer droplets by the sessile drop method, Soft Matter 17 (2021) 1655–1662.
[23] K.K. Jangra, An experimental study for multi-pass cutting operation in wire electrical discharge machining of WC-5.3% Co composite, Int. J. Adv. Manuf. Technol. 76 (2015) 971–982.
[24] D. Jauffrès, O. Lame, G. Vigier, F. Doré, T. Douillard, Sintering mechanisms involved in high-velocity compaction of nascent semicrystalline polymer powders, Acta Mater. 57 (2009) 2550–2559.
[25] S.Z. Jiang, Z.N. Guo, Y. Deng, H.S. Dong, X.Y. Li, J.W. Liu, Effect of pulse frequency on the one-step preparation of superhydrophobic surface by pulse electrodeposition, Appl. Surf. Sci. 458 (2018) 603–611.
[26] X.X. Qiao, X.J. Zhang, P. Chen, Y. Tian, Y.G. Meng, Influences of micro-groove size on surface anisotropic wetting behaviors, Acta Phys. Sin. 69 (2020) 7.
[27] B.M. Lekube, W. Hermann, C. Burgstaller, Partially compacted polypropylene glass fiber non-woven composite: Influence of processing, porosity and fiber length on mechanical properties and modeling, Compos. Pt. A-Appl. Sci. Manuf. 135 (2020) 10.